Reversible Engineering of Topological Insulator Surface State Conductivity through Optical Excitation

Faji Xie^{1,*}, Zhen Lian^{2,*}, Shuai Zhang^{1,*}, Tianmeng Wang², Shengnan Miao², Zhiyong Song³, Zhe Ying¹, Xing-Chen Pan¹, Mingsheng Long¹, Minhao Zhang¹, Fucong Fei¹, Weida Hu³, Geliang Yu¹, Fengqi Song^{1,†}, Ting-Ting Kang^{3,‡}, and Su-Fei Shi^{2,4,§}

- 1. National Laboratory of Solid State Microstructures, School of Physics and Collaborative Innovation Center of Advanced Microstructures, Nanjing University, Nanjing 210093, China
- 2. Department of Chemical and Biological Engineering, Rensselaer Polytechnic Institute, Troy, New York 12810, USA
- 3. State Key Laboratory of Infrared Physics, Shanghai Institute of Technical Physics, Chinese Academy of Sciences, Shanghai 200083, China
- 4. Department of Electrical, Computer & Systems Engineering, Rensselaer Polytechnic Institute, Troy, New York 12180, USA

Despite the broadband response, limited optical absorption at a particular wavelength hinders the development of optoelectronics based on Dirac fermions. Heterostructures of graphene and various semiconductors have been explored for this purpose, while non-ideal interfaces often limit the performance. The topological insulator is a natural hybrid system, with the surface states hosting high-mobility Dirac fermions and the small-bandgap semiconducting bulk state strongly absorbing light. In this work, we show a large photocurrent response from a field effect transistor device based on intrinsic topological insulator Sn-Bi_{1.1}Sb_{0.9}Te₂S (Sn-BSTS). The photocurrent response is non-volatile and sensitively depends on the initial Fermi energy of the surface state, and it can be erased by controlling the gate voltage. Our observations can be explained with a remote photo-doping mechanism, in which the light excites the defects in the bulk and frees the localized carriers to the surface state. This photodoping modulates the surface state conductivity without compromising the mobility, and it also significantly modify the quantum Hall effect of the surface state. Our work thus illustrates a route to reversibly manipulate the surface states through optical excitation, shedding light into utilizing topological surface states for quantum optoelectronics.

^{*} These authors contributed equally.

[†] Corresponding author. Emails: songfengqi@nju.edu.cn.

^{*} Corresponding author. Emails: kang@mail.sitp.ac.cn.

[§] Corresponding author. Emails: shis2@rpi.edu.

Introduction

Dirac fermions [1, 2] with high mobility have been widely explored for electronic devices [3-5], and it was also proposed for optoelectronics for its broadband absorption [6, 7]. However, monolayer graphene only absorbs about 2.3% light in the visible to midinfrared regime [8, 9], limiting the possible applications. Various combinations of semiconductor and graphene heterostructures [10-14], therefore, have been explored to overcome this limitation, with the semiconductor absorbing light and the graphene hosting high mobility conducting channels. In these heterostructures, light excited carriers need to be transferred efficiently to the graphene layer, which are often constrained by non-ideal interfaces. Topological insulator (TI) [15-17], with its symmetry protected surface states and semiconducting bulk state, provides a natural hybrid structure to bypass this dilemma. The surface states of the TI possess spinpolarized linear dispersion [18, 19] that hosts massless Dirac fermions, similar to graphene but with spin degeneracy lifted. The bulk state of the topological insulator is a small bandgap semiconductor, which strongly absorbs light in the visible to midinfrared regime [20]. The superior electrical and optical properties render TI an ideal candidate for optoelectronics applications, such as photo-induced surface current [21-24], helical edge charge transport[25] and terahertz excitation [26-28]. However, the direct optical manipulation of the quantum transport behaviors of the topological surface state (TSS) is still lacking, because of the conductivity of TSS are often shadowed by the bulk conductivity due to unintentional doping.

Results and discussion

In this work, we investigate the photo-response of a field effector transistor (FET) based on intrinsic TI: Sn-Bi_{1.1}Sb_{0.9}Te₂S (Sn-BSTS). We found a large and non-volatile photocurrent response from the TI FET device, which arises from the effective doping of the TSS. The photocurrent response sensitively depends on the initial Fermi energy of the TSS, and the memory effect can be erased by a large gate voltage or raising the temperature. We further propose a remote doping mechanism, in which the light excites the defect states in the bulk and the trapped carriers are freed to the TSS. The resulting photodoping leads to the greatly modified the conductivity of TSS observed in the experiments. Our interpretation is further confirmed by the quantum magneto-transport measurements under the continuous illumination of light. The photodoping modifies the quantum Hall effect (QHE) in the TI FET by broadening and shifting the position of the quantum Hall conductance plateau. Our study shows the possibility of using light excitation as a new knob to manipulate the TSS of TI in the quantum Hall regime.

The TI FET device is schematically shown in figure 1(a). The TI flake is typically ~100 nm thick, placed on 300 nm thermal SiO₂ and gated by the silicon back gate (see Methods section). In dark, the electrical transport measurement of the device at 2 K clearly shows a bipolar behavior [figure 1(b), black curve], a signature of the TSS dominated transport. The optimized TI, Sn-BSTS, has been reported to have a mobility up to 10,277 cm²/Vs when the Fermi energy is tuned close to Dirac point [29]. The minimum conductivity of the device shown in figure 1 is ~ 4.5 G_0 , consistent with

previous report [30, 31]. The charge neutral point (CNP) of bottom TSS (\sim -5.5 V) is close to zero gate voltage, suggesting that the Fermi energy is not only in the bandgap but also very close to the Dirac point of the TSS, a result of minimum initial doping of the surface state. We then illuminate the device with a LED light source, with excitation power of 11 μ W and center wavelength of 945 nm. The resulting transfer curves with the light on maintain the bipolar behavior, suggesting that the transport is still dominated by the TSS (later also confirmed by quantum Hall measurements). Since the change of top TSS conductance is a constant, there are two major changes: (1) The CNP shifts from \sim 5.5 V to \sim -59.5 V; (2) the conductance slope becomes flatter [Fig. 1(b)]. The shift of CNP can be explained with the effective electron doping of the TSS upon optical excitation. Interestingly, under the optical excitation, the mobility of the surface states remains \sim 1800 cm²/Vs, same as the value obtained under dark condition (Fig. S6e). The flatter conductance vs gate voltage curve, however, is due to the decreased effective capacitance (Supplementary Information section 4).

These changes lead to a large photocurrent response, \sim -0.256 nA for both CNP (-5.5V) and gate voltage of 60 V, with a bias as small as \sim 3 mV. The photocurrent sign change is a natural consequence of photo-induced conductivity change of the TSS conductivity [figure 1(b)]. As shown in figure 1(b), the photocurrent is positive in region II (-25.0 V to 29.0 V) but negative in region I (29.0 V to 60.0 V) and III (-80.0 V to -25.0 V). Time-dependent photoconductivity measurement is also performed at fixed V_g to confirm the gate tunable transition between increased and deceased photo-induced conductivity

change (Supplementary Information section 3).

The gate voltage in figure 1(b) are swept from 60 to -80 V, as indicated by the arrow direction in figure 1(b). We further measure the transfer curves by sweeping the gate voltage on both directions. As shown in figure 1(c), in dark, the TI device shows a large hysteresis (black curve). Previously, the origins of the hysteresis in graphene and transition metal dichalcogenides FETs have been systematically studied and are attributed to trap states or mobile ions inside gate dielectric layers or water molecules trapped in graphene/oxide interfaces [32-35], which tend to be suppressed either in high vacuum or at low temperature [33-35], opposite to our observations of hysteresis at the temperature of 2 K. Our controlled device of h-BN gated TI devices show similar behavior of hysteresis upon light excitation (Supplementary Information section 7), which indicates that the hysteresis is an intrinsic properties of Sn-BSTS. Threedimensionally distributed charged impurities in the bulk state of TI give rise to the hysteresis of the TSS transport [36-38]. Interestingly, the hysteresis decreases as the excitation power increases and eventually disappears for the LED power of 11 µW [red curves in figure 1(c)].

The transfer curves of our device measured at different excitation powers are shown in figure 2(a). As the excitation power increases, the effective doping of the TSS increases, as evidenced by the shift of CNP. The amount of photodoping can be estimated from the shift of CNP by the expression, where $c_{\rm eff}$ is effective gate capacitance per unit area,

 $\Delta V_{\rm CNP}$ is the shift of CNP and e is the electron charge constant (Supplementary Information section 5). It can be found that the photodoping of TSS increases as a function of the LED power at low excitation power, while it saturates around 5.6 μ W. At the excitation power 11 μ W, the effective electron doping is $=3.3\times10^{11}\,\mathrm{cm}^{-2}$, which roughly correspond to a Fermi energy shift of 26.8 meV.

Interestingly, the minimum conductivity remains roughly the same (~4.5 G₀) for different optical excitation powers. This insensitive dependence of the minimum conductivity on increased charge impurity scattering center on the surface was reported in graphene [30, 39] and TI [40] experimentally, which were further confirmed by theory of Dirac fermions [41-43]. The light excitation, therefore, could be controlled to investigate the minimum conductivity of Dirac fermions of TI.

The photodoping effect is non-volatile and persists after turning off the light (Supplementary Information section 3). Further, the photodoping effect sensitively depend on the initial Fermi level of the TSS. To check this behavior in detail, we take a different approach of illuminating the second device [figure 2(b)]. Here, we turn on the optical excitation of 11 μ W at one particular gate voltage. We then turn off the light and sweep the gate voltage to -80 V. The data for different initial gate voltages are shown in figure 2(b). Compared with the transfer curve taken in the dark [dashed black line in figure 2(b)], the flashed illumination at the gate voltage of 60 V shows a transfer curve of a p-doped TSS. With the decrease of the initial gate voltage that we flash the

light, the CNP voltage keeps decreasing, and the transfer curve eventually turns to one corresponding to the n-doped TSS.

All our observations can be explained with a remote photo-doping mechanism. Shown in figure 2(c-e), there are a distribution defect states in the bulk that are close to the Direct point of TSS in energy, which act as donor-like and acceptor-like states (only show two discrete levels for simplicity in the schematics) to the TSS that can be activated through light. Upon illumination, the trapped electron or hole can be activated to the high energy conduction band or valence band, and then relax to the low energy state, either the TSS or the original defect states. When the initial gate voltage is at 60 V for the flashed light excitation, TSS is n-doped. Optically excited electron would prefer to relax to the donor-like defects state and then be stuck due to the large binding energy of the localized state. However, the optically excited holes from the acceptorlike defects can transfer to TSS, leaving behind negatively charged defects that effectively gate the TSS to be more p-doped compared with the original TSS not exposed to light. Once the holes transferred to the TSS, they quickly relax energy and cannot go back to the defect states, leading to the non-volatile change after the light is turned off. As the initial gate voltage for the flashed light excitation decreases, TSS is less n-doped initially. The Fermi energy is lower than some of the donor-like defect states, and optically excited electrons start to transfer to TSS. As a result, the TSS start to be more n-doped after the optical excitation. For the initial gate voltage close to CNP [figure 2(d)], almost all optically excited electrons and holes can transfer to TSS. There are more donor-like defect states the acceptor-like defect states, and as a results, there are more positively charged defects left behind after the carrier transfer, which act as the effective gating that n-dope the TSS. Finally, as the initial gate voltage was tuned to -30 V, light excited holes transfer to TSS start to get blocked, while all the optically excited electron can be transferred to the TSS, leading to even more n-doped TSS after the flashed optical excitation.

It is worth noting that there are two ways to erase the non-volatile doping effect (Supplementary Information section 2). One is to sweep $V_{\rm g}$ below -80 V or above 60 V. This suggests that at corresponding Fermi energies, the carrier have enough energy to go back to defect states and then get trapped there. Considering the effective capacitance, this suggests that the defect states are distributed around the Dirac point by \pm (30-50meV) (Supplementary Information section 8). The other way is to raise the temperature to be over 100 K and then cool the device down to 2 K. This suggests that the thermal excitation of ~ 10 meV is enough to facilitate the carrier go back to defect states, which is more effective than tuning the gate voltage. The reason is that, according to the Fermi distribution, there is a small population of carrier with the kinetic energy larger than 10 meV. Considering the fast tunneling time and finite time of electrical transport measurement (10s'), even a finite tunneling probability would drive all carriers back to defect states during our measurement. The origin of these defects is beyond the scope of this work, but certainly warrants future exploration considering the intense interest in intrinsic TIs.

Notably, with this model, we can also explain the decrease of the gate efficiency upon light illumination which flattens the transfer curve [figure 1(b)], which is also later confirmed by QHE measurement (Supplementary Information section 4). Since the optical excitation creates empty defect states, the carriers induced by the gate voltage have to fill the defect states before filling the TSS.

Magneto-transport measurements have been employed to unambiguously demonstrate QHE of the TSS [29, 31, 44-46] and associated nontrivial Berry phase [47]. The conductance of TI arises from the parallel top and bottom surface states. Under high magnetic fields, both top and bottom surface states get into quantum Hall regime with vanishing G_{xx} and quantized $G_{xy} = e^2/h$, where $=_{top} +_{bottom} = (N_{top} + 1/2) + (N_{bottom} + 1/$ 1/2), $N_{\text{top(bottom)}}$ indicates the filling half-integer Landau levels for top (bottom) surface. Here we measure the Hall conductivity of the TI device with and without the continuous optical excitation. The gate voltage dependence of longitudinal conductance G_{xx} , Hall conductance G_{xy} , as well as two-terminal conductance $G_{2\text{-term}}$ are measured at $B=14~\mathrm{T}$ and T = 2 K, all exhibiting the characteristics of TSS-dominated transport [figure 3(ac)]. In dark, G_{xy} shows two well-developed plateaus, which correspond to the total Landau filling factor 0 and -1, respectively [figure 3(b)]. The transition between the two plateaus, accompanied by one peak in G_{xx} , is located very close to the CNP [figure 3(c)], indicating the filling of zeroth Landau level of the bottom surface. Such observation is in good agreement with previous studies [29, 31, 46] and can be explained by half-integer QHE conductivity from both the top and bottom surface states: while the filling factor of the top surface $_{top}$ remains as -1/2, $_{bottom}$ can be tuned from - 1/2 to 1/2 by the back-gate voltage.

We further examine the influence of the photodoping effect on the QHE. Upon the continuous LED light illumination with the power 11 μ W, it is evident from figure 3(b) that the QHE plateaus of $-e^2/h$ of G_{xy} shifts to the negative gate voltage and also broadens in width, and the corresponding G_{xx} peak exhibit a shift in position as well. As shown in figure 3(c), the zeroth Landau level (LL) has shifted from -6.6 V to -65.8 V, which is the same as the shift of CNP for the device 1 as shown in figure 1(b). These results show that, upon light illumination, the transport of the TI device shows QHE of an electron-doped TSS, as schematically shown in figure 3(e).

The analysis of QHE is given by renormalization group flow diagrams (RGFDs) [48, 49] as shown in figure 3(d) and Methods section, which indicates complete Landau quantization of the bottom TSS. For RGFDs under light illumination, the sets of converging points can be observed with G_{xy} pointing to 0 and $-e^2/h$. It is clearly that all the RGFDs under different excitation power show continuous evolution of Landau quantization and reach an integer. It indicates that TSS is still a well-protected 2D electron system under light illumination. We further confirmed that, through analysis of weak anti-localization, transport dissipation from bulk can be ignored (Supplementary Information section 6).

Conclusion

In summary, we report the observation of photo-doping of the TSS of a FET device based on Sn-BSTS, and the effects can be sensitively tuned by the optical excitation power and gate voltage. The gate voltage controlled non-volatile photodoping of TSS promise applications in novel memory devices. Since the photodoping arise from the activation of the defect states in bulk and their coupling to the TSS, our study also inspires future work on defect engineering in TI bulk state for optoelectronics based on TSS. Further, the optical excitation of these defects can be utilized as a new knob to explore quantum transport of TSS such as the origin of minimum conductivity and optically controllable QHE.

Methods

Crystal growth and device fabrication. High-quality Sn-BSTS crystals were grown by melting elements of Bi, Sb, Te, S in a molar ratio of 1.1:0.9:2:1 and a small quantity of Sn at 750 °C for 24h in evacuated vacuum quartz tubes, followed by cooling to room temperature naturally. The crystal with a low bulk carrier density can be cleaved easily. With mechanical exfoliation, the Sn-BSTS flakes were transferred onto SiO₂/Si substrates, which was then fabricated as gated Hall-bar devices by photolithography, electron-beam evaporation and standard lift-off techniques.

Transport measurements and analysis. The transport measurements were carried out by a physical property measurement system at low temperatures down to 2 K with a

magnetic field up to 14 T. We measured the resistances by standard lock-in amplifiers (SR830) with a low-frequency (13.33Hz) excitation current of 1uA (Keithley 6221). A direct current source (Keithley 2400) was used to power the LED. The conductivities are calculated by and, and are dependent on the parameters such as temperature, magnetic field, back-gate voltage and light illumination. The RGFDs allow extraction of two sets of converging points in the (G_{xy} , G_{xx}) space. Here the temperature and magnetic field are fixed, and the RGFDs are plotted with different light excitation power for different back-gate voltages. Each curve in the RGFDs is under a fixed light illumination power (dark as the excitation power of zero), which corresponding to different doping and can be viewed as different Fermi levels.

Supporting Information

Supporting Information is available from the Wiley Online Library or from the author.

Acknowledgements

We gratefully acknowledge the financial support of the National Key R&D Program of China (2017YFA0303203), the National Natural Science Foundation of China (91622115, 11522432, 11574217, U1732273, U1732159, 61822403, 11874203, 11904165 and 11904166), the Natural Science Foundation of Jiangsu Province (BK20160659 and BK20190286), the Fundamental Research Funds for the Central Universities, and the opening Project of the Wuhan National High Magnetic Field Center. We also acknowledge the assistance of the Nanofabrication and Characterization Center at the Physics College of Nanjing University. Z.L., T.W., S.M. and S.-F. Shi acknowledges the support from AFOSR through Grant FA9550-18-1-0312, ACS PRF through Grant 59957-DNI10, NYSTAR through Focus Center-NY–RPI Contract C150117, and NSF through Career Grant DMR-1945420.

Author contributions

FS conceived the work. FX fabricated the devices and performed the transport measurement as assisted by SZ. X.-C.P. and F. F. prepared the bulk crystal. ZS, ML, WH, ZL, S.-F.S. and T.-T.K. provided the conditions of light experiment. FX, ZL, TW, SM and S.-F.S. proposed the photo doping mechanism model. FX, ZL, S.-F.S and FS co-wrote the paper. SZ, MZ, and GLY participated in the discussions. All authors commented on the manuscript.

Additional information

Correspondence and requests for materials should be addressed to FS.

Competing financial interests

The authors declare no competing financial interests.

References

- [1] Novoselov K S *et al* 2005 Two-dimensional gas of massless Dirac fermions in graphene *Nature* 438 197-200
- [2] Zhou S Y et al 2006 First direct observation of Dirac fermions in graphite Nat. Phys. 2 595-9
- [3] Bonaccorso F, Sun Z, Hasan T and Ferrari A C 2010 Graphene photonics and optoelectronics *Nat. Photon.* 4 611-22
- [4] Avouris P 2010 Graphene: Electronic and Photonic Properties and Devices Nano Lett. 10 4285-94
- [5] Bao Q and Loh K P 2012 Graphene Photonics, Plasmonics, and Broadband Optoelectronic Devices *Acs Nano* 6 3677-94
- [6] Liu M et al 2011 A graphene-based broadband optical modulator Nature 474 64-7
- [7] Bao Q et al 2011 Broadband graphene polarizer Nat. Photon. 5 411-5
- [8] Nair R R et al 2008 Fine structure constant defines visual transparency of graphene Science 320 1308
- [9] Mak K F, Sfeir M Y, Wu Y, Lui C H, Misewich J A and Heinz T F 2008 Measurement of the Optical Conductivity of Graphene *Phys.Rev. Lett.* 101
- [10] Qiao H *et al* 2015 Broadband Photodetectors Based on Graphene-Bi2Te3 Heterostructure *Acs Nano* 9 1886-94
- [11] Liu C-H, Chang Y-C, Norris T B and Zhong Z 2014 Graphene photodetectors with ultra-broadband and high responsivity at room temperature *Nat. Nanotech.* 9 273-8
- [12] Wang X, Cheng Z, Xu K, Tsang H K and Xu J-B 2013 High-responsivity graphene/silicon-heterostructure waveguide photodetectors *Nat. Photon.* 7 888-91
- [13] Zhang W et al 2014 Ultrahigh-Gain Photodetectors Based on Atomically Thin Graphene-MoS2 Heterostructures Sci. Rep. 4 03826
- [14] Miao J et al 2015 High-Responsivity Graphene/InAs Nanowire Heterojunction Near-Infrared Photodetectors with Distinct Photocurrent On/Off Ratios Small 11 936-42
- [15] Moore J E 2010 The birth of topological insulators Nature 464 194-8
- [16] Hasan M Z and Kane C L 2010 Colloquium: Topological insulators Rev. Mod. Phys. 82 3045-67
- [17] Qi X-L and Zhang S-C 2011 Topological insulators and superconductors *Rev. Mod. Phys.* 83 1057-110
- [18] McIver J W, Hsieh D, Steinberg H, Jarillo-Herrero P and Gedik N 2012 Control over topological insulator photocurrents with light polarization *Nat. Nanotech.* 7 96-100

- [19] Pan Y *et al* 2017 Helicity dependent photocurrent in electrically gated (Bi1-x Sb x)2Te3 thin films *Nat. Commun.* 8 1037
- [20] Zhang H, Zhang X, Liu C, Lee S-T and Jie J 2016 High-Responsivity, High-Detectivity, Ultrafast Topological Insulator Bi2Se3/Silicon Heterostructure Broadband Photodetectors *Acs Nano* 10 5113-22
- [21] Braun L et al 2016 Ultrafast photocurrents at the surface of the three-dimensional topological insulator Bi2Se3 Nat. Commun. 7 13259
- [22] Duan J et al 2014 Identification of Helicity-Dependent Photocurrents from Topological Surface States in Bi2Se3 Gated by Ionic Liquid Sci. Rep. 4 4889
- [23] Kastl C, Karnetzky C, Karl H and Holleitner A W 2015 Ultrafast helicity control of surface currents in topological insulators with near-unity fidelity *Nat. Commun.* 6 6617
- [24] Seifert P, Vaklinova K, Kern K, Burghard M and Holleitner A 2017 Surface State-Dominated Photoconduction and THz Generation in Topological Bi2Te2Se Nanowires *Nano Lett.* 17 973-9
- [25] Dolcini F, Iotti R C, Montorsi A and Rossi F 2016 Photoexcitation of electron wave packets in quantum spin Hall edge states: Effects of chiral anomaly from a localized electric pulse *Phys.Rev. B* 94 165412
- [26] Yao J, Shao J, Wang Y, Zhao Z and Yang G 2015 Ultra-broadband and high response of the Bi2Te3-Si heterojunction and its application as a photodetector at room temperature in harsh working environments *Nanoscale* 7 12535-41
- [27] Olbrich P *et al* 2014 Room-Temperature High-Frequency Transport of Dirac Fermions in Epitaxially Grown Sb2Te3- and Bi2Te3-Based Topological Insulators *Phys. Rev. Lett.* 113 096601
- [28] Yao X, Tokman M and Belyanin A 2014 Efficient nonlinear generation of THz plasmons in graphene and topological insulators *Phys. Rev. Lett.* 112 055501
- [29] Xie F *et al* 2019 Phase transition and anomalous scaling in the quantum Hall transport of topological-insulator Sn–Bi1.1Sb0.9Te2S devices *Phys. Rev. B* 99 081113
- [30] Chen J H, Jang C, Adam S, Fuhrer M S, Williams E D and Ishigami M 2008 Charged-impurity scattering in graphene *Nat. Phys.* 4 377-81
- [31] Xu Y et al 2014 Observation of topological surface state quantum Hall effect in an intrinsic three-dimensional topological insulator *Nat. Phys.* 10 956-63
- [32] Schedin F *et al* 2007 Detection of individual gas molecules adsorbed on graphene *Nat. Mater.* 6 652-5
- [33] Qiu H, Pan L, Yao Z, Li J, Shi Y and Wang X 2012 Electrical characterization of back-gated bilayer MoS2 field-effect transistors and the effect of ambient on their performances *Appl. Phys. Lett.* 100 123104

- [34] Wang H M, Wu Y H, Cong C X, Shang J Z and Yu T 2010 Hysteresis of Electronic Transport in Graphene Transistors *Acs Nano* 4 7221-8
- [35] Late D J, Liu B, Matte H S S R, Dravid V P and Rao C N R 2012 Hysteresis in Single-Layer MoS2 Field Effect Transistors *Acs Nano* 6 5635-41
- [36] Skinner B, Chen T and Shklovskii B I 2013 Effects of bulk charged impurities on the bulk and surface transport in three-dimensional topological insulators *Journal of Experimental and Theoretical Physics* 117 579-92
- [37] Beidenkopf H *et al* 2011 Spatial fluctuations of helical Dirac fermions on the surface of topological insulators *Nat. Phys.* 7 939-43
- [38] Borgwardt N *et al* 2016 Self-organized charge puddles in a three-dimensional topological material *Phys. Rev. B* 93 245149
- [39] Yan J and Fuhrer M S 2011 Correlated charged impurity scattering in graphene *Phys. Rev. Lett.* 107 206601
- [40] Kim D *et al* 2012 Surface conduction of topological Dirac electrons in bulk insulating Bi2Se3 *Nat. Phys.* 8 459-63
- [41] Hwang E H, Adam S and Sarma S D 2007 Carrier transport in two-dimensional graphene layers *Phys. Rev. Lett.* 98 186806
- [42] Adam S, Hwang E H, Galitski V M and Das Sarma S 2007 A self-consistent theory for graphene transport *Proceedings of the National Academy of Sciences of the United States of America* 104 18392-7
- [43] Culcer D, Hwang E H, Stanescu T D and Das Sarma S 2010 Two-dimensional surface charge transport in topological insulators *Phys. Rev. B* 82 155457
- [44] Yoshimi R *et al* 2015 Quantum Hall effect on top and bottom surface states of topological insulator (Bi1-xSbx)2Te3 films *Nat. Commun.* 6 6627
- [45] Koirala N *et al* 2015 Record Surface State Mobility and Quantum Hall Effect in Topological Insulator Thin Films via Interface Engineering *Nano Lett.* 15 8245-9
- [46] Zhang S *et al* 2017 Anomalous quantization trajectory and parity anomaly in Co cluster decorated BiSbTeSe2 nanodevices *Nat. Commun.* 8 977
- [47] Hsieh D *et al* 2009 A tunable topological insulator in the spin helical Dirac transport regime *Nature* 460 1101-U59
- [48] Checkelsky J G *et al* 2014 Trajectory of the anomalous Hall effect towards the quantized state in a ferromagnetic topological insulator *Nat. Phys.* 10 731-6
- [49] Khmelnitskii D E 1983 QUANTIZATION OF HALL CONDUCTIVITY Jetp Letters 38 552-6

Figures

Figure 1. Light induced doping of surface states of an intrinsic topological insulator. (a) Schematic of topological insulator Sn-BiSbTeS(1.1:0.9:2:1) based phototransistor. Purple lines indicate the topological surface states (b) Comparison of Transfer curves for dark and 11 μ W light illumination at 2 K. (c) Transfer curves with hysteresis under different optical excitation power. The arrows indicate the scanning direction.

Figure 2. Controllable photodoping of the topological surface state. (a) Transfer curves for different optical excitation powers at 2 K. (b) Transfer curves displaying non-volatile photodoping effect for different initial gate voltages under which the flashed light illumination occur. (c)-(e) Schematics showing the photodoping mechanism for initially n-doped (c), intrinsic (d), and p-doped TSS.

Figure 3. QHE of TSS upon light illumination. (a) Back gate voltage dependent two-terminal conductance, $G_{2\text{-term}}$, at 14T for different optical excitation powers. The dashed lines indicate QHE states with index v. The inset shows the measurement configuration. The arrows show direction of sweeping back-gate voltage. (b) and (c) are G_{xy} (b) and G_{xx} (c) as a function of the back gate voltage at 14T for different light illumination power, respectively. (d) The renormalization-group flow diagram (RGFD) in (G_{xy} , G_{xx}) space. Each curve in the RGFD correspond to one fixed light illumination power (Dark, 0.01 μW, 0.1 μW, 0.5 μW, 1.1 μW, 5.6 μW, and 11 μW). (e) Schematics showing the Fermi energy of the TSS with respect to the LLs for both dark and upon illumination, with the back gate voltage set at -30 V.

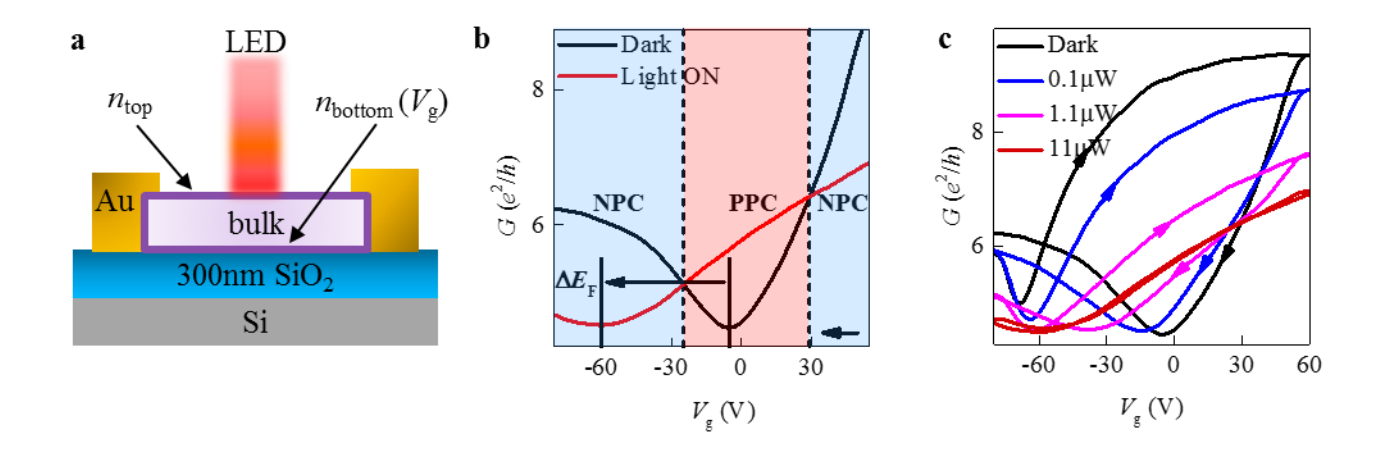


Figure 1

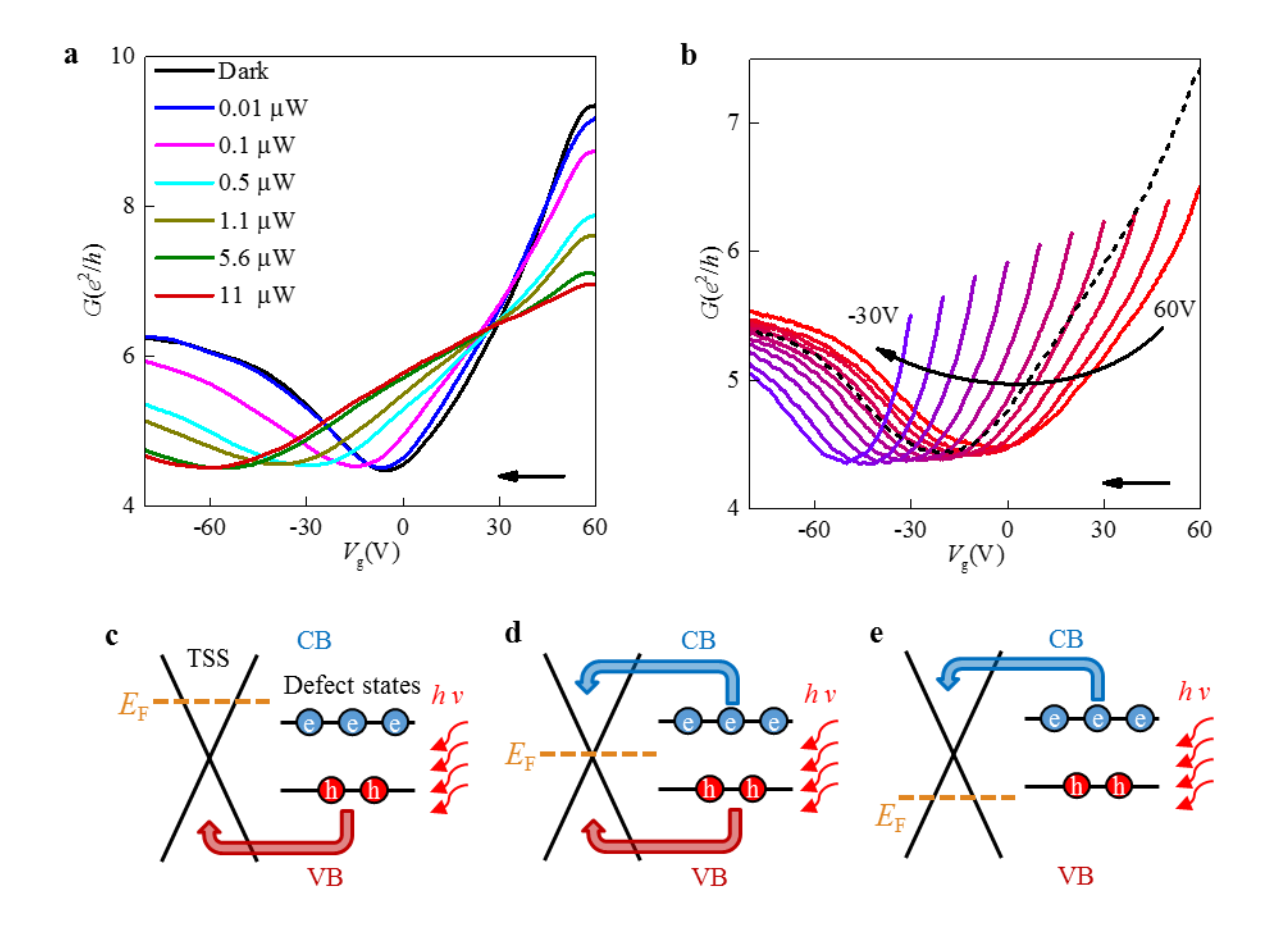


Figure 2

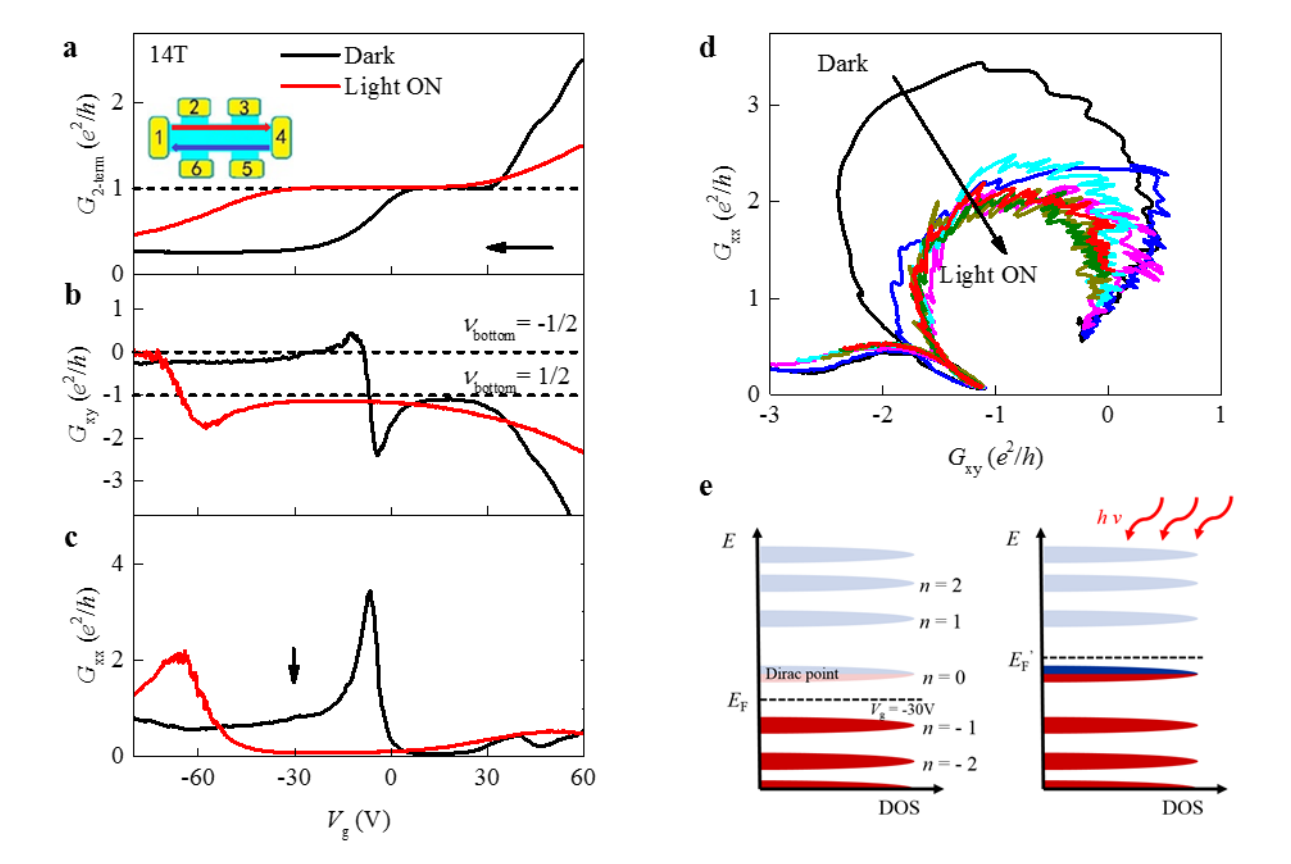


Figure 3